Research Article | Vol. 30, No. 20 / 26 Sep 2022 / Optics Express 36500
Optics EXPRESS

Near-perfect (>99%) dual-band absorption in the visible using ultrathin semiconducting gratings

TAO GONG[1,2,*] AND JEREMY N. MUNDAY[1]

[1]Department of Electrical and Computer Engineering, University of California, Davis, Davis, CA 95616, USA
[2]Department of Materials Science and Engineering, University of California, Davis, Davis, CA 95616, USA
[*]taogong@ucdavis.edu

Abstract: Electromagnetic perfect absorption entails impedance-matching between two adjacent media, which is often achieved through the excitation of photonic/plasmonic resonances in structures such as metamaterials. Recently, super absorption was achieved using a simple bi-layer configuration consisting of ultrathin lossy films. These structures have drawn rising interest due to the structural simplicity and mechanical stability; however, the relatively broadband absorption and weak angular dependence can limit its versatility in many technologies. In this work, we describe an alternative structure based on an ultrathin semiconducting (Ge) grating that features a dual-band near-perfect resonant absorption (99.4%) in the visible regime. An angular-insensitive resonance is attributed to strong interference inside the ultrathin grating layer, akin to the resonance obtained with a single ultrathin planar film, while an angular-sensitive resonance shows a much narrower linewidth and results from the diffraction-induced surface mode coupling. With an appropriately designed grating period and thickness, strong coherent coupling between the two modes can give rise to an avoided-crossing in the absorption spectra. Further, the angular-insensitive resonance can be tuned separately from the angularly sensitive one, yielding a single narrow-banded absorption in the visible regime and a broadband absorption resonance that is pushed into the near-infrared (NIR). Our design creates new opportunities for ultra-thin and ultra-compact photonic devices for application in technologies including image sensing, structural color-filtering and coherent thermal light-emission.

1. Introduction

Near-unity absorption of electromagnetic energy (*i.e.* perfect absorption, or PA) has been extensively explored and exploited in a variety of applications such as solar energy harvesting, thermal emitters for thermophotovoltaics (TPV), chemical and bio-sensing, optical modulation, spectral filtering, and wireless communications [1–3]. In principle, PA in a device is the combinatorial result of a surface with impedance-matched media (*e.g.*, air and the structure), which suppresses energy reflection, and subsequent energy absorption or dissipation in materials of the underlying structure. To achieve impedance-matching, photonic/plasmonic resonant structures are often employed to modify the surface impedance. Typical resonant structures utilized include metal-dielectric-metal (MDM)-based Fabry-Perot cavities [4–7], diffraction gratings of metallic or dielectric materials [8,9], dielectric nanostructure resonators [10–12], and metamaterials [13–16]. Alternatively, non-resonant structures are another category of (near) perfect absorbers. They usually feature a low effective permittivity, such as multilayer stacks composed of alternating metallic and dielectric thin films [17,18] and carbon nanotube forests [19]. Yet, many of these structures demand sophisticated nano-fabrication steps. Moreover, the absorption mostly occurs in the metallic components and is subsequently dissipated as Ohmic loss, which is undesired in many applications for energy-harvesting and optoelectronics.

Over the past decade, a novel bi-layer structure consisting of an ultrathin highly-absorbing dielectric film (*e.g.*, semiconductors) on an opaque substrate (*e.g.*, metals) has drawn increasing

#470617 https://doi.org/10.1364/OE.470617
Journal © 2022 Received 14 Jul 2022; revised 20 Aug 2022; accepted 31 Aug 2022; published 21 Sep 2022

Optics EXPRESS

attention owing to advantages such as the structural simplicity and compactness, mechanical flexibility, and direct photocarrier generation [20,21]. PA in this configuration results from strong optical interference due to the nontrivial interface phase-shift, which allows the total phase accumulation to reach zero with a thickness much smaller than a quarter of the wavelength ($d \ll \frac{\lambda}{4}$), in combination with the high loss of the material, giving rise to strong optical attenuation. Following the originally proposed structure of an ultrathin Ge film on Au [22], a series of analogous absorber structures composed of alternative materials have flourished utilizing other semiconducting materials (*e.g.*, Si, GaAs and InGaAs) [23–26] or phase-change materials (*e.g.*, VO_2) [27,28] for the ultrathin film coating layer and alternative metals (*e.g.*, Ag, Al, Cu, Cr, Ti) [29–32] or distributed Bragg stacks for the substrate [33]. These structures exhibit near-perfect absorption (NPA) in various wavelength regimes from visible (VIS) to far-infrared (FIR). On the other hand, the absorption is typically broadband due to the intrinsically high loss (*i.e.*, low quality-factor) of the ultrathin film. In addition, the angular dependence of absorption is weak as a result of the extremely small thickness and large refractive index of the film [22,30]. These characteristics hamper their applicability in certain technologies.

In such bi-layer structures, the optical properties of the top ultrathin absorbing layer play a vital role in determining the absorption spectra. A homogeneous film is structurally simple yet the performance is constrained by the availability of materials with the appropriate optical response. Structural modifications to the top ultrathin film can somewhat overcome this issue by introducing geometry and dimension as additional tuning parameters. Though scarce, some research in this direction has been reported. For instance, the Ge film has been replaced with a dense array of Ge ultrathin nanobeams or a Ge photonic crystal (PhC), which has exhibited resonantly enhanced absorption in the visible regime attributed to the excited resonance of individual Ge nanobeam or the PhC mode [34,35]. Alternatively, a top layer comprised of an ultrathin a-Si metafilm with sub-wavelength patterning has shown tunable absorption, as the effective refractive index of the metafilm can be readily adjusted by the duty cycle of the patten [36]. Nevertheless, the demonstrated absorption spectra in these configurations are still relatively broadband and angle-insensitive, and variants to these structures and the resulted PA characteristics remain underexplored.

In this work, we devise an alternative structure based on an ultrathin Ge grating on top of an optically thick Au film and systematically investigate the absorption characteristics. This structure exhibits a dual-band NPA in the visible regime: The broadband angularly insensitive resonance is controlled predominantly by the grating layer thickness and is almost invariant with respect to the grating width or gap size. This resonance is attributed to the strong interference inside the Ge layer, hence it is present for both transverse magnetic (TM) and transverse electric (TE) polarizations, akin to the NPA effect in a smooth Ge ultrathin film. On the contrary, the narrowband NPA absorption is angular-sensitive and depends critically on the grating period, with a redshifted resonance at a larger incidence angle. This resonance results from the diffraction-induced surface mode coupling and exists only for TM polarization. With appropriate geometrical parameters, the two resonant modes can coherently couple with each other, giving rise to the archetypal "avoided-crossing" pattern in the absorption spectra. Alternately, the angular-insensitive resonant mode can be tuned out of the visible regime by thickening the grating layer, featuring a single narrowband absorption in the VIS. The maximum absorption achieved is 99.4% with a grating thickness of 60 nm and a grating period of 300 nm. Our design provides a new route for achieving tailorable NPA utilizing ultrathin semiconducting nanostructures and may find significant applications in pertinent technologies such as structural color filtering, image sensing and coherent thermal emission.

Optics EXPRESS

2. Results and discussion

The schematic in Fig. 1(a) illustrates the structure under consideration. An ultrathin Ge grating layer (15 nm-thick) is placed atop an Au substrate (150 nm-thick). Light fields with either TM or TE polarization (***H*** field or ***E*** field along the y direction, parallel to the grating strips) impinge from the top at a particular angle of incidence (with respect to the z axis). The Ge grating width w and the gap size g between the grating strips are both 150 nm.

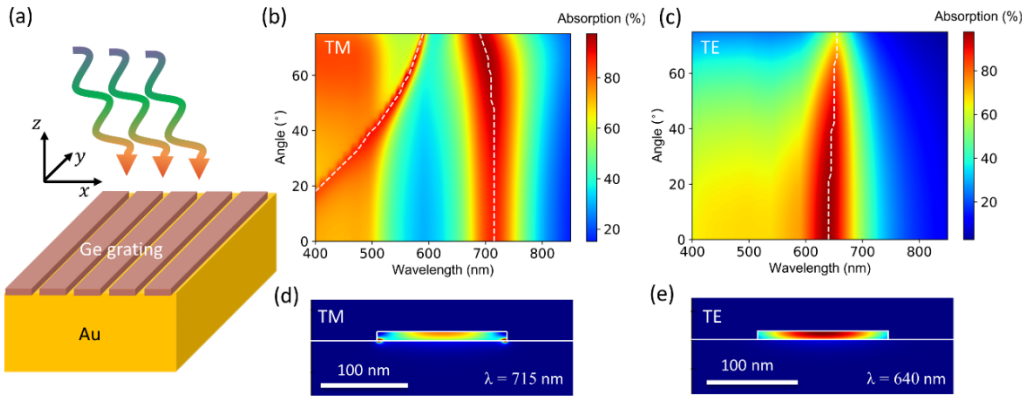

Fig. 1. Absorption characteristics for the Ge ultrathin grating-based structure. (a): Schematic of the bi-layer configuration: ultrathin Ge grating is placed on an Au substrate (150 nm thick). The grating thickness, grating width and the gap **size** between grating strips are d = 15 nm, w = 150 nm and g = 150 nm, respectively. (b) and (c): Contour plots of the absorption spectra with respect to incidence angle under (b) TM-polarized and (c) TE-polarized illumination. For TM-polarization, a dual-band resonant NPA is observed: an angular-insensitive resonance (maximum absorption ~96.9%) at wavelengths of about 715 nm, and a highly angular-sensitive resonance (maximum absorption ~97.3%) over a shorter wavelength range (400-600 nm). For TE-polarization, only an angular-insensitive resonance (maximum absorption ~97.6%) at wavelengths of about 640 nm exists. The white dashed lines represent the peak absorption wavelengths at varying incidence angles. (d) and (e): Absorption cross-sectional profiles for (d) TM-polarization and (e) TE-polarization at normal incidence at their respective resonance wavelengths of 715 nm and 640 nm.

As shown in Fig. 1(b)–(c), a relatively broadband absorption is located in the wavelength range of 600-750 nm for both polarizations. With normal incidence, the linewidth for this absorption mode is about 120 nm, and the resonant wavelength is insensitive to the incidence angle. As the incidence angle increases from 0° to 75°, the resonant wavelength blueshifts slightly from 715 nm to 695 nm for TM polarization, and redshifts from 640 nm to 655 nm for TE polarization. The maximum absorption for the two polarizations is 96.9% at the incidence angle of 70° and 97.6% at normal incidence, respectively. These abovementioned absorption properties resemble those in a smooth Ge ultrathin film-coated Au substrate reported in literature [22]. As such the resonance can be analogously attributed to the interference induced by phase accumulation across the ultrathin film and upon interface reflection. The cross-sectional resonant absorption profiles shown in Fig. 1(d)–(e) also indicate this effect. The absorption is distributed across the entire ultrathin grating layer, and the strong field attenuation in the lateral directions results from the high loss of Ge. For TM polarization, significant absorption also occurs at the corners of the grating strips due to the lightning rod effect [37,38]. Overall, the resonant absorption takes place predominantly inside the grating layer (72% for TM and 86.4% for TE), whereas Au substrate only accounts for 15.4% and 11.2% for TM and TE, respectively. We note that an absorption of about 60%−70% occurs for wavelengths between 400–500 nm. This absorption

Optics EXPRESS

is attributed to the high loss of Ge in this wavelength range, signified by the large value of its imaginary part of the refractive index, k (see Supplement 1, Fig. S1(a)). Figure S1(b) shows this material-intrinsic absorption band also takes place in a 15 nm-thick Ge film atop an Au substrate for TM polarization without the grating structure.

A notable distinction between the two polarizations is the presence of an extra narrowband (linewidth 40-50 nm), highly angular-sensitive NPA resonance emerging at shorter wavelengths (400-600 nm) only for the TM-polarized illumination. This resonant absorption is ascribed to the diffraction-induced surface mode coupling. Further discussions on this mode will be detailed in the following sections.

The influences of the lateral size parameters of the grating (*e.g.*, grating width w and gap size g) on the angularly insensitive absorption band are examined. As shown in Fig. 2(a), with a fixed grating width (150 nm), the absorption peak is slightly redshifted from 700 nm to 730 nm as g increases from 50 nm to 300 nm under normal incidence with TM polarization. Concurrently, the peak absorption amplitude drops modestly from 97.2% to 72.4%. However, the resonant absorption for TE polarization exhibits a subtle blueshift from 645 nm to 640 nm with increasing g (see Supplement 1, Fig. S2 and S3). This behavior indicates the capacitive coupling between the neighboring grating strips for TM polarization is nontrivial in determining the resonance. Meanwhile, the variation of the grating width exerts minimal influence on the resonance. The absorption peak wavelength slightly shifts from 730 nm with $w =$ 50 nm to 720 nm with a $w =$ 250 nm for a fixed gap size of 200 nm (Fig. 2(b)). This behavior is another manifestation that the resonance is not along lateral dimensions but rather is due to the thickness of individual grating strips. In both scenarios (*i.e.*, either smaller g or larger w), the absorption increases with larger filling fractions of the Ge material per grating period, which can be understood intuitively as more absorbing material being utilized.

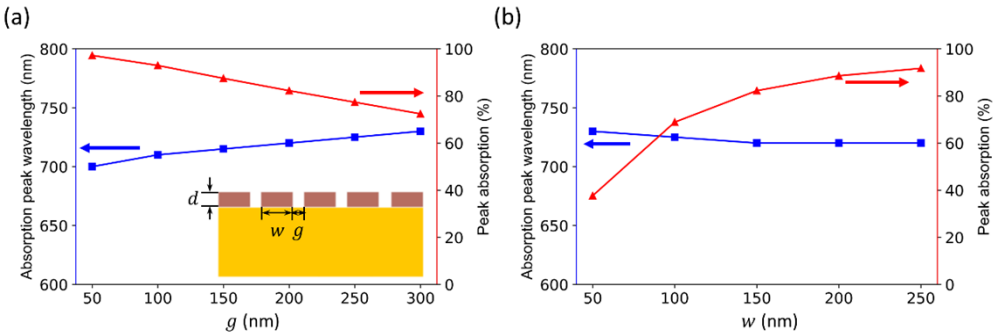

Fig. 2. Grating lateral size affects the angularly insensitive resonant absorption under TM-polarized illumination at normal incidence. The grating thickness is $d =$ 15 nm. (a) Peak absorption (red) and the corresponding wavelengths (blue) for different gap sizes g between grating strips. The grating width is fixed at $w =$ 150 nm. With increasing g, the absorption peak redshifts from 700 nm to 730 nm due to the weaker coupling between the neighboring grating strips. The peak absorption amplitude decreases from 97.2% to 72.4% due to the decreased volume of Ge. (b) Peak absorption and the corresponding wavelengths for different grating widths w. The gap size is fixed at $g =$ 200 nm. With increasing w, the absorption peak wavelength barely shifts, and the peak absorption amplitude gradually increases with increasing w due to the increased amount of Ge.

As the phase accumulation across the Ge layer scales with the grating thickness d, the angular-insensitive resonance mode redshifts with thicker grating layers (Fig. 3). With a sufficiently thick grating layer (>30 nm), the resonance can be pushed into the near-IR regime (at a wavelength > 850 nm). Concomitantly, the angularly insensitive absorption is much less dependent on d.

Optics EXPRESS

Therefore, only this absorption band exists in the visible regime with a sufficiently large thickness, which differs dramatically from the dual-band absorption with an ultrathin grating layer (Fig. 3(a) versus Fig. 3(b)–(c)).

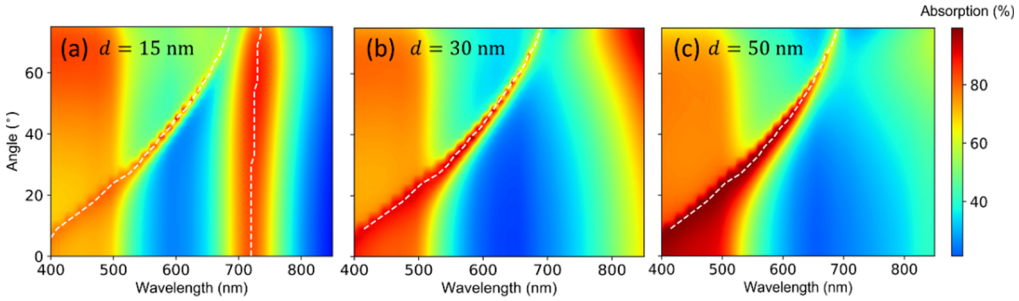

Fig. 3. Contour plots of absorption spectra with respect to incidence angle under TM-polarized illumination. The Ge layer thickness is (a) $d =$ 15 nm, (b) $d =$ 30 nm and (c) $d =$ 50 nm, while the lateral size parameters of the grating are fixed, ($w =$ 150 nm and $g =$ 200 nm). The resonance wavelengths of the angular-insensitive absorption band shifts substantially to the longer wavelengths (into the NIR regime) with a thicker Ge layer, indicating the resonance is primarily due to the interference effect within the ultrathin film. For the 50 nm-thick grating layer, only the grating-induced angular-sensitive absorption band remains within the visible regime.

The narrowband, angularly sensitive resonant absorption for the TM polarization can be described via a grating effect. The presence of the Ge grating changes the in-plane wavevector of the incident light field through diffraction, providing additional momentum for exciting the surface mode propagating at the substrate surface. The phase-matching condition and the resulted absorption enhancement takes place when:

$$\beta = k_0 \sin(\theta) \pm j\frac{2\pi}{a} \tag{1}$$

where β is the wavenumber of the surface mode, θ is the angle of incidence and a is the grating period ($a = w + g$). Consequently, a strong angular dependence of the absorption is induced. Further, such dependence arising from the collective response of the grating lattice is only determined by the grating period and is not affected much by the size of individual grating strip (*e.g.*, grating width w and thickness d), as seen in Fig. 3 and Fig. S4 in Supplement 1. The dependence of the resonance wavelength on the incidence angle for additional grating layer thicknesses ranging from 15 nm to 100 nm, all of which overlap, are shown in Fig. 4(a).

While the angular dependence of the resonant wavelength is immune to the grating thickness, the total absorption amplitude of the resonance is highly dependent upon it. Figure 4(b) shows how the peak absorption varies with incidence angle for different grating thicknesses. Interestingly, the peak absorption over all incidence angles for this resonance mode on average varies nonmonotonically with the thickness. An optimal thickness of ~ 60 nm results in a total absorption of 99.4%. The inset of Fig. 4(b) shows the cross-sectional absorption profile at the resonance wavelength of 540 nm at an incidence angle of 30° for a 60 nm-thick grating. Compared to the angularly insensitive resonance mode, a significantly larger fraction of absorption is distributed at the Au surface due to the surface mode. The near-unity total absorption is a result of comparable contributions from the grating layer and the substrate. As shown in Fig. 4(c), grating layers that are too thick or too thin give rise to weaker coupling into the surface mode and hence more absorption results in the Ge grating layer, and the total absorption is slightly reduced from near-unity.

Optics EXPRESS

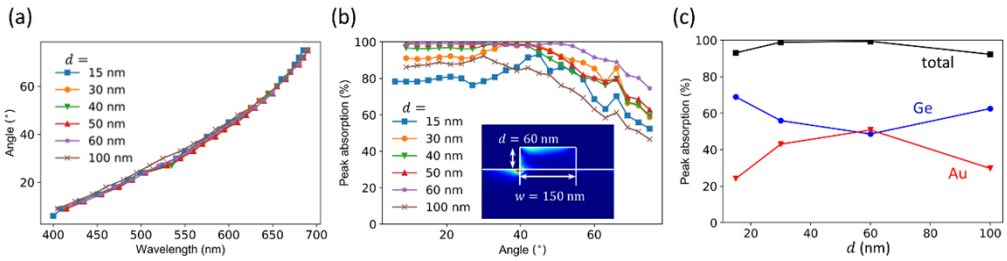

Fig. 4. Effect **of** grating thickness on the angularly sensitive resonant absorption under TM-polarized illumination. The grating width and the gap size are $w =$ 150 nm and $g =$ 200 nm, respectively. (a) Absorption peak wavelength and (b) peak absorption amplitude as a function of incidence angle for different Ge layer thicknesses d. Near-unity absorption (99.4%) is achieved with $d =$ 60 nm. Inset: absorption cross-sectional profile at an incidence angle of 30° for the resonance wavelength of 540 nm. The strong absorption at the Au substrate surface indicates the grating-induced surface mode coupling. (c) Peak absorption in the entire structure (black), Ge grating (blue), and Au substrate (red) for a few different grating thicknesses d. Optimal total absorption occurs with a thickness where the grating and the substrate absorb comparable amount of the incident energy.

Because the angular-dependence of the grating diffraction-induced resonant absorption is only determined by the grating period, appropriate selection of the period can in principle modify the angular-dependence such that it interacts with the broadband angular-insensitive absorption band. Figure 5(a) illustrates that the angular-dependence curve bends to lower slopes with increasing grating period, in line with Eq. (1). As such, the grating period-controlled resonance shows great tunability of its angular dependence. For instance, the resonance wavelength (~610 nm) can be tuned out of the material's intrinsic lossy region (400-500 nm) with a grating period of 600 nm (w = 300 nm and g = 300 nm) at normal incidence to retain the narrow linewidth, as shown in Fig. S5. However, when the gap size is in the range of 250-300 nm, the angularly dependent resonance is shifted away from the angular-insensitive absorption band, causing the angularly insensitive absorption band to shift towards longer wavelengths. This behavior forms an avoided-crossing patten, which is indicative of coherent coupling of the two resonant modes. As seen in Fig. 5(b), the coupling takes place around an incidence angle of 50° for a gap size of 250 nm. Note that the coupling strength, signaled by the splitting of the two modes around the otherwise crossing point, is not profound. This behavior is a result of the low quality-factor of the grating thickness-induced resonance mode due to the highly absorbing nature of the material.

The characteristic dual-band absorption and its remarkable tunability can allow for extensive technological applications in a variety of fields, including spectral color filters, image sensors, high-performance solar cells, selective thermal emitters, multi-wavelength photo-thermal devices and multiplexing detector arrays [39–43]. For instance, a good selective thermal emitter used in a thermophotovoltaic (TPV) system should feature an emissivity (equal to absorptivity by Kirchhoff's law [44]) profile that matches the PV cell bandgap E_g. Specifically, absorption of low-energy photons ($E<E_g$) in the emitter should be strongly suppressed whereas the high-energy photons ($E>E_g$) are preferentially absorbed within a certain bandwidth above E_g to optimize the power conversion efficiency [45,46]. In this regard, our structure as an emitter can satisfy such needs through the tuning of the angular insensitive broadband resonance to be right above E_g. Moreover, the second resonance can further enhance the above-bandgap emissivity of the emitter, facilitating more charge-carrier generation in the PV cell and hence enhancing the overall output power [47], allowing for tuning between maximum power output and maximum efficiency. Alternatively, our structure can be used to create directional thermal emission for greater control

Optics EXPRESS

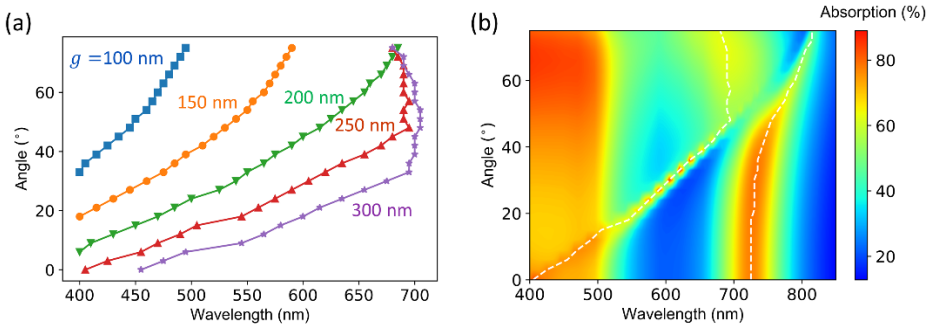

Fig. 5. Effect of grating period on the angular-sensitive resonant absorption under TM-polarized illumination. The grating thickness and width are $d =$ 15 nm and $w =$ 150 nm, respectively. (a) Absorption peak wavelength as a function of incidence angle for different gap sizes g between grating strips. (b) Contour plot of the absorption spectra with respect to incidence angle, with $g =$ 250 nm. The avoided-crossing pattern indicates the coherent coupling between the two resonant modes.

of heat regulation or for spectrum splitting solar technologies. We further note that compared with many other multi-band absorbers based on two or more local electrical and/or magnetic resonances, which complicates the structure and its fabrication, our design would only entail a single-layer one-dimensional patterning with much more flexibility and simplicity in a compact size.

3. Conclusions

In summary, we designed and systematically investigated an ultrathin Ge grating-based bi-layer dual-band perfect absorber in the visible wavelength regime, with a maximum absorption of 99.4%. The broadband angularly insensitive resonance is attributed to the strong interference inside the Ge grating ultrathin layer and can be controlled by the grating thickness. Meanwhile, the narrowband angularly sensitive mode results from the diffraction-induced surface mode coupling and the associated angular-dependence hinges on the grating period. The two resonant modes can coherently couple with one another, which yields an archetypal avoided-crossing pattern in the absorption spectra. Conversely, the dual-band absorption can also be adapted to a single band in the visible regime with a thicker grating layer as the angular-insensitive mode can be controlled to move into the NIR wavelength range. Our work creates new opportunities for utilizing ultrathin lossy material-based photonic devices for applications such as image sensing, structural color-filtering, and coherent thermal light emission.

Funding. Defense Advanced Research Projects Agency (HR00112190008).

Disclosures. The authors declare no conflicts of interest.

Data availability. Data underlying the results presented in this paper are not publicly available at this time but may be obtained from the authors upon reasonable request.

Supplemental document. See Supplement 1 for supporting content.

References

1. C. M. Watts, X. Liu, and W. J. Padilla, "Metamaterial Electromagnetic Wave Absorbers," Adv. Mater. **24**(23), OP98–OP120 (2012).
2. Y. Cui, Y. He, Y. Jin, F. Ding, L. Yang, Y. Ye, S. Zhong, Y. Lin, and S. He, "Plasmonic and metamaterial structures as electromagnetic absorbers," Laser Photonics Rev. **8**(4), 495–520 (2014).
3. Y. Ra'di, C. R. Simovski, and S. A. Tretyakov, "Thin Perfect Absorbers for Electromagnetic Waves: Theory, Design, and Realizations," Phys. Rev. Appl. **3**(3), 037001 (2015).

Optics EXPRESS

4. Z. Li, S. Butun, and K. Aydin, "Large-area, lithography-free super absorbers and color filters at visible frequencies using ultrathin metallic films," ACS Photonics **2**(2), 183–188 (2015).
5. W. Pengdi, Z. Xianghua, and W. Jue, "AlN film-based Fabry–Perot cavity resonance enhanced absorption," J. Nanophotonics **15**(1), 1–11 (2021).
6. H. Shin, M. F. Yanik, S. Fan, R. Zia, and M. L. Brongersma, "Omnidirectional resonance in a metal–dielectric–metal geometry," Appl. Phys. Lett. **84**(22), 4421–4423 (2004).
7. Z. Li, E. Palacios, S. Butun, H. Kocer, and K. Aydin, "Omnidirectional, broadband light absorption using large-area, ultrathin lossy metallic film coatings," Sci. Rep. **5**(1), 15137 (2015).
8. K. Ito, T. Matsui, and H. Iizuka, "Thermal emission control by evanescent wave coupling between guided mode of resonant grating and surface phonon polariton on silicon carbide plate," Appl. Phys. Lett. **104**(5), 051127 (2014).
9. J. Le Perchec, P. Quémerais, A. Barbara, and T. López-Ríos, "Why Metallic Surfaces with Grooves a Few Nanometers Deep and Wide May Strongly Absorb Visible Light," Phys. Rev. Lett. **100**(6), 066408 (2008).
10. J. Tian, H. Luo, Q. Li, X. Pei, K. Du, and M. Qiu, "Near-Infrared Super-Absorbing All-Dielectric Metasurface Based on Single-Layer Germanium Nanostructures," Laser Photonics Rev. **12**(9), 1800076 (2018).
11. X. Liu, J. Zhou, H. Zhang, H. Zhong, J. Shang, and Z. Liu, "Ultra-thin Semiconductor/Metal Resonant Superabsorbers," Plasmonics **14**(6), 1427–1433 (2019).
12. S. Bao, G. Zheng, and Y. Ma, "Total absorption for an ultrathin silicon grating within the low-loss mid-infrared window," Opt. Mater. **108**, 110431 (2020).
13. N. I. Landy, S. Sajuyigbe, J. J. Mock, D. R. Smith, and W. J. Padilla, "Perfect metamaterial absorber," Phys. Rev. Lett. **100**(20), 207402 (2008).
14. J. Hao, J. Wang, X. Liu, W. J. Padilla, L. Zhou, and M. Qiu, "High performance optical absorber based on a plasmonic metamaterial," Appl. Phys. Lett. **96**(25), 251104 (2010).
15. K. Aydin, V. E. Ferry, R. M. Briggs, and H. A. Atwater, "Broadband polarization-independent resonant light absorption using ultrathin plasmonic super absorbers," Nat. Commun. **2**(1), 517 (2011).
16. K. Chen, T. D. Dao, S. Ishii, M. Aono, and T. Nagao, "Infrared Aluminum Metamaterial Perfect Absorbers for Plasmon-Enhanced Infrared Spectroscopy," Adv. Funct. Mater. **25**(42), 6637–6643 (2015).
17. T.-A. Chen, M.-J. Yub, Y.-J. Lu, and T.-J. Yen, "Ultra-broadband, lithography-free, omnidirectional, and polarization-insensitive perfect absorber," Sci. Rep. **11**(1), 5173 (2021).
18. J. Zhou, X. Chen, and L. J. Guo, "Efficient Thermal–Light Interconversions Based on Optical Topological Transition in the Metal-Dielectric Multilayered Metamaterials," Adv. Mater. **28**(15), 3017–3023 (2016).
19. H. Shi, J. G. Ok, H. Won Baac, and L. Jay Guo, "Low density carbon nanotube forest as an index-matched and near perfect absorption coating," Appl. Phys. Lett. **99**(21), 211103 (2011).
20. L. J. Krayer, J. Kim, J. L. Garrett, and J. N. Munday, "Optoelectronic Devices on Index-near-Zero Substrates," ACS Photonics **6**(9), 2238–2244 (2019).
21. L. J. Krayer, J. Kim, and J. N. Munday, "Near-perfect absorption throughout the visible using ultra-thin metal films on index-near-zero substrates [Invited]," Opt. Mater. Express **9**(1), 330–338 (2019).
22. M. A. Kats, R. Blanchard, P. Genevet, and F. Capasso, "Nanometre optical coatings based on strong interference effects in highly absorbing media," Nat. Mater. **12**(1), 20–24 (2013).
23. F. F. Schlich and R. Spolenak, "Strong interference in ultrathin semiconducting layers on a wide variety of substrate materials," Appl. Phys. Lett. **103**(21), 213112 (2013).
24. J.-T. Liu, X.-H. Deng, W. Yang, and J. Li, "Perfect light trapping in nanoscale thickness semiconductor films with a resonant back reflector and spectrum-splitting structures," Phys. Chem. Chem. Phys. **17**(5), 3303–3308 (2015).
25. S.-T. Yen and P.-K. Chung, "Far-infrared quasi-monochromatic perfect absorption in a thin GaAs film on gold," Opt. Lett. **40**(16), 3877–3880 (2015).
26. A. Heßler, I. Bente, M. Wuttig, and T. Taubner, "Ultra-Thin Switchable Absorbers Based on Lossy Phase-Change Materials," Adv. Opt. Mater. **9**(24), 2101118 (2021).
27. M. A. Kats, D. Sharma, J. Lin, P. Genevet, R. Blanchard, Z. Yang, M. M. Qazilbash, D. N. Basov, S. Ramanathan, and F. Capasso, "Ultra-thin perfect absorber employing a tunable phase change material," Appl. Phys. Lett. **101**(22), 221101 (2012).
28. H. Kocer, S. Butun, E. Palacios, Z. Liu, S. Tongay, D. Fu, K. Wang, J. Wu, and K. Aydin, "Intensity tunable infrared broadband absorbers based on VO2 phase transition using planar layered thin films," Sci. Rep. **5**(1), 13384 (2015).
29. J. Park, J.-H. Kang, A. P. Vasudev, D. T. Schoen, H. Kim, E. Hasman, and M. L. Brongersma, "Omnidirectional Near-Unity Absorption in an Ultrathin Planar Semiconductor Layer on a Metal Substrate," ACS Photonics **1**(9), 812–821 (2014).
30. D. Liu, H. Yu, Y. Duan, Q. Li, and Y. Xuan, "New Insight into the Angle Insensitivity of Ultrathin Planar Optical Absorbers for Broadband Solar Energy Harvesting," Sci. Rep. **6**(1), 32515 (2016).
31. S. S. Mirshafieyan, H. Guo, and J. Guo, "Zeroth Order Fabry–Perot Resonance Enabled Strong Light Absorption in Ultrathin Silicon Films on Different Metals and Its Application for Color Filters," IEEE Photonics J. **8**(5), 1–12 (2016).
32. V. Medvedev, V. Gubarev, E. Zoethout, and N. Novikova, "Interference-Enhanced Absorption of Visible and Near-Infrared Radiation in Ultrathin Film Coatings," IEEE Photonics Technol. Lett. **33**(22), 1242–1245 (2021).

Optics EXPRESS

33. X.-L. Zhang, J.-F. Song, X.-B. Li, J. Feng, and H.-B. Sun, "Anti-reflection resonance in distributed Bragg reflectors-based ultrathin highly absorbing dielectric and its application in solar cells," Appl. Phys. Lett. **102**(10), 103901 (2013).
34. P. Molet, J. L. Garcia-Pomar, C. Matricardi, M. Garriga, M. I. Alonso, and A. Mihi, "Ultrathin Semiconductor Superabsorbers from the Visible to the Near-Infrared," Adv. Mater. **30**(9), 1705876 (2018).
35. S. J. Kim, P. Fan, J.-H. Kang, and M. L. Brongersma, "Creating semiconductor metafilms with designer absorption spectra," Nat. Commun. **6**(1), 7591 (2015).
36. K.-T. Lee, J.-Y. Jang, S. J. Park, C. Ji, S.-M. Yang, L. J. Guo, and H. J. Park, "Angle-Insensitive and CMOS-Compatible Subwavelength Color Printing," Adv. Opt. Mater. **4**(11), 1696–1702 (2016).
37. M. Urbieta, M. Barbry, Y. Zhang, P. Koval, D. Sánchez-Portal, N. Zabala, and J. Aizpurua, "Atomic-Scale Lightning Rod Effect in Plasmonic Picocavities: A Classical View to a Quantum Effect," ACS Nano **12**(1), 585–595 (2018).
38. M. Hrtoň, A. Konečná, M. Horák, T. Šikola, and V. Křápek, "Plasmonic Antennas with Electric, Magnetic, and Electromagnetic Hot Spots Based on Babinet's Principle," Phys. Rev. Appl. **13**(5), 054045 (2020).
39. K. Chen, R. Adato, and H. Altug, "Dual-Band Perfect Absorber for Multispectral Plasmon-Enhanced Infrared Spectroscopy," ACS Nano **6**(9), 7998–8006 (2012).
40. Z. Zhang, Z. Yu, Y. Liang, and T. Xu, "Dual-band nearly perfect absorber at visible frequencies," Opt. Mater. Express **8**(2), 463–468 (2018).
41. H. Xu, L. Hu, Y. Lu, J. Xu, and Y. Chen, "Dual-Band Metamaterial Absorbers in the Visible and Near-Infrared Regions," J. Phys. Chem. C **123**(15), 10028–10033 (2019).
42. S. Feng, Y. Zhao, and Y.-L. Liao, "Dual-band dielectric metamaterial absorber and sensing applications," Results Phys. **18**, 103272 (2020).
43. Z. Yan, X. Lu, K. Chen, Z. Lv, X. Pu, C. Tang, and P. Cai, "Ultranarrow Dual-Band Perfect Absorption in Visible and Near-infrared Regimes Based on Three-Dimensional Metamaterials for Ultrahigh-Sensitivity Sensing," J. Lightwave Technol. **39**(22), 7217–7222 (2021).
44. G. Neuer, "Spectral and total emissivity measurements of highly emitting materials," Int. J. Thermophys. **16-16**(1), 257–265 (1995).
45. T. Burger, C. Sempere, B. Roy-Layinde, and A. Lenert, "Present Efficiencies and Future Opportunities in Thermophotovoltaics," Joule **4**(8), 1660–1680 (2020).
46. S. Hassan, C. F. Doiron, and G. V. Naik, "Optimum selective emitters for efficient thermophotovoltaic conversion," Appl. Phys. Lett. **116**(2), 023903 (2020).
47. N.-P. Harder and P. W. rfel, "Theoretical limits of thermophotovoltaic solar energy conversion," Semicond. Sci. Technol. **18**(5), S151–S157 (2003).